DOI: 10.1016/j.apor.2019.101994

A lumped parameter model to explain the cause of the hysteresis in OWC-Wells turbine systems for wave energy conversion

Tiziano Ghisu[a], Francesco Cambuli[a], Pierpaolo Puddu[a], Irene Virdis[a], Mario Carta[a], Fabio Licheri[a]

[a] *Department of Mechanical, Chemical and Materials Engineering. University of Cagliari, via Marengo 2, 09123 Cagliari, Italy*

Abstract

A Wells turbine is an axial-flow turbine consisting of a rotor usually with symmetric (uncambered) blades staggered at a 90 degree angle relative to the machine's axis. This turbine is used within oscillating water column systems: during its normal operation, the blades experience a continuous change in incidence angle, that according to many authors is at the origin of a hysteresis in its force coefficients. Aerodynamic hysteresis in rapidly moving airfoils is a well-known phenomenon, but happens only at non-dimensional frequencies significantly larger than the ones encountered in Wells turbines. This work presents a re-examination of the two phenomena, that shows the unlikeliness of the presence of any aerodynamic hysteresis in Wells turbines. A simple yet effective lumped parameter analysis is used to prove how the real cause of the hysteresis is to be found in a different phenomenon. Results are compared to experiments and CFD analyses for the same problem, with an excellent agreement.

Keywords: OWC systems, Wells turbines, hysteresis, wave energy conversion

Nomenclature

Acronyms

CFD computational fluid dynamics

Article accepted in Applied Ocean Research

LEV leading edge vortex

LPM lumped parameter model

OWC oscillating water column

Dimensional properties

a speed of sound [m s^{-1}]

A cross area [m^2]

c blade chord [m]

f frequency [s^{-1}]

F_x turbine axial force [kg m s^{-2}]

L turbine duct length [m]

M_1 mass of air in the chamber [kg]

h_1 air chamber height [m]

p pressure [kg $m^{-1}s^{-2}$]

r_m blade midspan radius [m]

r_t blade tip radius [m]

t time [s]

T turbine torque [kg m^2 s^{-2}]

U blade speed [m s^{-1}]

U_∞ free-stream velocity [m s^{-1}]

V axial velocity [m s^{-1}]

Δp turbine pressure drop [kg m^{-1} s^{-2}]

ρ air density [kg m^{-3}]

ω turbine rotational speed [s^{-1}]

Ω piston angular frequency [s^{-1}]

Ω_n natural angular frequency [s^{-1}]

Non-dimensional properties

A, B, C, D coefficients of second order equation

c_d drag coefficient

c_l lift coefficient

c_m pitching moment coefficient

c_x turbine axial force coefficient

$c_{x,\phi}$ slope of c_x vs. ϕ curve

f_a non-dimensional turbine reactance

G transfer function

j imaginary unit

k non-dimensional (or reduced) frequency

M Mach number

P^* pressure drop coefficient

Re Reynolds number

t^* non-dimensional time

T^* torque coefficient

γ ratio of specific heats

ϕ_p piston-based flow coefficient

ϕ_l local flow coefficient

ρ^* non-dimensional density

σ turbine solidity

ξ_a phase shift due to turbine aerodynamics

ξ_{owc} phase shift due to OWC

ξ_{tot} total phase shift (sum of OWC and turbine)

ζ damping ratio

Subscripts and superscripts

0 amplitude

1 air chamber

2 turbine duct

a turbine duct outlet section

f turbine duct inlet section

l local

p piston

t tangential direction

x axial direction

1. Introduction

A Wells turbine is an axial-flow turbine consisting of a rotor usually with symmetric (uncambered) blades staggered at a 90 degree angle relative to machine's axis. This turbine is used within oscillating water column (OWC) systems, which convert the sea-wave motion into a bi-directional flow of air. The Wells turbine transforms the energy of the flow of air into mechanical energy, by means of the aerodynamic forces that are generated on the blades by the relative air motion. Schematics of OWC system and Wells turbine are given in Figure 1.

As the mass-flow passing through the turbine is alternate and periodic, the blades experience a continuous variation in incidence angle, i.e. they operate under dynamic conditions. Several authors have discussed the presence of a *hysteretic loop* when representing turbine performance as a function of

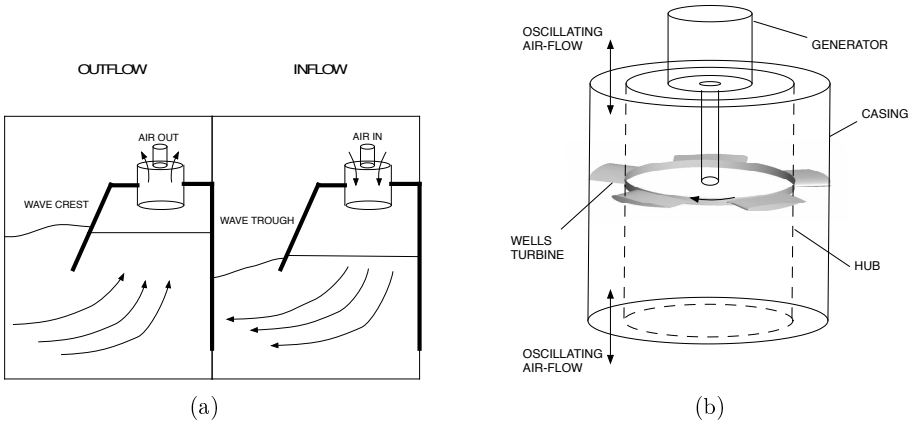

(a) (b)

Figure 1: OWC system (a) and Wells turbine (b)

the flow coefficient: aerodynamic forces acting on the blades were found to be larger during the deceleration phase (when the mass-flow through the turbine is decreasing) than during the acceleration phase (when it is increasing).

The presence of hysteresis was first discovered in experimental studies conducted on laboratory devices, where a piston moving inside a large cylinder was used to replicate the dynamic operating conditions typical of OWC-installed turbines [1, 2, 3, 4], and on full-scale systems [5]. In other studies [6, 7, 8, 9], the hysteresis appeared negligible. Puddu *et al.* [8, 9], in particular, highlighted how the hysteresis disappears when turbine performance is represented as a function of flow parameters measured in the proximity of the rotor.

The (generally accepted) explanation on the origin of the hysteresis was found by means of numerical (CFD) simulations, conducted on a domain consisting of a passage of the annular duct housing the turbine (i.e. air chamber and moving piston were not simulated). Kinoue *et al.* [10] attributed the difference in performance between acceleration and deceleration phases to the interaction of the blade circulation with trailing edge vorticity, shed by the blade due to the variation in flow incidence and opposite in sign during the two phases. The same explanation is given in other papers by the same research group (among many others [11, 12, 13, 14, 15, 16, 17]). The presence of dynamic effects in Wells turbines was also the focus of the recent numerical investigations by [18, 19, 20, 21, 22, 23], who gave essentially very similar explanations.

Numerical models have often been derived for the study of OWC systems: among these, wave-to-wire models analyze the energy conversion from the sea waves to the generator using conservation laws expressed in terms of ordinary differential equations [24, 25]. It should be noted that many of these studies discuss the presence of a delay between the displacement of the water level inside the OWC chamber and the mass-flow passing through the duct [26, 27, 28, 29, 30]. It is surprising how this information was not used in experiments that focused on the turbine performance under dynamic conditions [1, 2, 3, 4], to isolate the performance of the turbine from that of the OWC.

This work presents a re-examination of the cause of the hysteresis in Wells turbines, or, more appropriately, in OWC systems, by means of a simple yet very effective lumped parameter model (LPM). Section 2 presents a brief survey of the large literature available on oscillating airfoils, which highlights how, at least for this problem, dynamic effects, and hence hysteresis, are negligible at the non-dimensional frequencies typical of Wells turbines operation. Section 3 summarizes some recent research of interest to this work and introduces the LPM that will be used to explain the real cause of the hysteresis. Section 4 compares the results produced when applying the proposed model to the experimental setup of [4], and finally Section 5 summarizes the findings of this work.

2. Hysteresis in rapidly moving airfoils and wings

Several authors [10, 12, 17, 23] have compared the hysteresis in OWC-turbine systems to the hysteresis in oscillating airfoils. This aspect deserves some clarifications, as important similarities exist, as well as fundamental differences.

As highlighted in Section 1, the incidence of the flow on a Wells turbine changes continuously during its normal operation. This is similar to what happens in rapidly moving airfoils (pitching or plunging), a phenomenon that has been widely studied since the 1930s [31], given its importance in rotating machinery (wind turbines, compressors and helicopter rotors) [32] and animal propulsion (insects, birds, and fish) [33]. Significant efforts have been devoted to the study of this problem by NASA in the 1970s and 1980s [34, 35, 36, 37, 38], although several aspects are still at present under investigation [39, 40, 41, 42, 43, 44, 45].

A clear explanation of the causes of the hysteresis in rapidly moving airfoils is given by Ericsson and Reding [46]. The problem is governed by 3 distinct phenomena:

a. the interaction of wake vorticity with the airfoil circulation (opposite and concordant in sign during pitch-up and pitch-down, respectively), which determines a time-lag and hence an effective incidence lower during pitch-up and higher during pitch-down, responsible for a counter-clockwise loop in aerodynamic performance plots ($c_l - \alpha$, $c_d - \alpha$, and $c_m - \alpha$).
b. the moving wall determines an energization of the boundary layer, that is able to withstand a larger pressure gradient before separation, with the effect of an increase in stall angle.
c. the generation of a leading edge vortex (LEV), associated with a discontinuous change in circulation (i.e. flow separation) that interacts with the blade suction surface causing, during its passage, a sharp suction peak and a temporary increase in lift. After the passage of the LEV, the airfoil experiences a sudden drop in lift and an increase in drag and pitching moment.

The magnitude of these phenomena depends mainly on the non-dimensional (or reduced) frequency k, which is a ratio of the characteristic times of flow passage and airfoil motion [34, 36].

$$k = \frac{\pi f c}{U_\infty} \tag{1}$$

In equation (1), f is the frequency of oscillation (pitching or plunging), c the airfoil's chord, and U_∞ the free-stream velocity. Reynolds number and amplitude of the oscillation are also important, but mainly for determining whether the airfoil exceeds, during its movement, the static stall angle, which in turns determines the formation of the LEV. If the static stall angle is not exceeded, Reynolds number and oscillation amplitude are of secondary importance [47]. Mach number effects are also minimal, provided that shock waves are absent [35].

When the airfoil movement does not cause flow separation (i.e. the static stall angle is not exceeded), only the first phenomenon (a) can be present. The vorticity shed by the blade interacts with the blade circulation causing a time-lag in the attainment of the static forces and hence a counter-clockwise hysteretic loop. At reduced frequencies below 0.08, the phase angle produced

by shed vorticity is well approximated by the linear relation $\xi_a = -3k$ [46]. It can be easily verified that non-dimensional frequencies well above 10^{-2} are required for the hysteresis to become noticeable [48].

If the static stall angle is exceeded, there will be both a delay of stall (with respect to static performance) caused by boundary layer improvement (b), and the generation of the LEV, that is convected by the free-stream velocity and therefore interacts with the airfoil for a fraction of the period proportional to k. The effect is a clockwise loop in the $c_l - \alpha$ curve, caused by the increase in suction due to the passage of the LEV on the suction surface and by a delayed reattachment of the boundary layer after stall. These effects start to be important only for $k > 4 \times 10^{-3}$ [35, 38]. The co-existence of wake vorticity interaction and LEV formation can generate, at high non-dimensional frequencies, the appearance of a bow in the airfoil's aerodynamic curves [36, 37].

Wells turbines operate at very low non-dimensional frequencies (lower than 10^{-3} [4, 18, 23]), well below the value that is necessary to produce hysteresis in rapidly pitching or plunging airfoils [35, 38, 46], especially if the stall angle is not exceeded. The difference between the non-dimensional frequencies of Wells turbine and oscillating airfoils is an aspect that has been overlooked in previous Wells turbine research, and persuaded the authors of this article to question the traditional explanation of the cause of the hysteresis in Wells turbines.

3. Revisiting the cause of the hysteresis: a lumped parameter model

The absence of aerodynamic hysteresis in oscillating airfoils, and other turbomachinery, at the non-dimensional frequencies typical of Wells turbine operation, convinced the authors of this article that this topic, and its generally accepted explanation, deserved a careful reinvestigation.

In an experimental setup similar to the one of Setoguchi [4], Puddu *et al.* [8, 9] verified that the renowned hysteresis was only present when performance was plotted as a function of flow parameters measured in the chamber, while it was significantly reduced (below the experimental uncertainty) when performance was presented as a function of the local flow coefficient, measured in the vicinity of the turbine. Ghisu *et al.* [49, 50, 51, 52, 53, 54] analyzed the problem using the same geometrical dimensions and numerical

assumptions of [10, 11, 12, 13, 14, 15, 16, 17, 23], and verified how the alleged aerodynamic hysteresis was caused only by an incorrect choice of the temporal discretization. Excluding the presence of any temporal discretization errors is of fundamental importance, especially in a study that deals with hysteresis, where numerical phase errors could be confused with a real hysteresis, leading to wrong physical conclusions [55, 56, 57].

By means of CFD simulations for the full experimental setup (moving piston, chamber, and turbine) Ghisu *et al.* [50, 51] showed how the hysteresis in the experiment [4] was caused by the compressibility of the air mass in the OWC chamber. Only if turbine performance had been represented as a function of the local flow coefficient, as in the experiments of Puddu *et al.* [8, 9], dynamic effects in the turbine could have been isolated from dynamic effects in the overall OWC, and they would probably have been found to be negligible [50].

It should be noted that the presence of a delay between the displacement of the water column inside the OWC chamber and the mass-flow passing through the duct has often been discussed in wave-to-wire models derived for the analysis of OWC systems [26, 27, 58, 28, 59, 29, 24, 60, 30]. This information seems to have been ignored in the experiments from Setoguchi [4], where the water displacement was replaced by a mechanical piston in order to focus the attention on the performance of the turbine under representative unsteady operating conditions. The same information was also ignored in the following CFD analyses [10, 11, 12, 13, 14, 15, 16, 17], which did not account for the delay between piston movement and turbine mass-flow before discussing the presence of any aerodynamic hysteresis.

The objective of this work is to show how a model simpler than CFD (especially in terms of computational cost, could have been used to investigate the cause of the hysteresis in the experiment of Setoguchi *et al.* [4]. The model derived in this work is called lumped parameter model (LPM), to differentiate it from distributed models such as CFD, which make use of partial differential equations to analyze the problem. LPMs are often used in the analysis of dynamic systems, such as pressure transducers, which are composed of a (variable size) volume connected to the measurement point through a pneumatic line (a narrower tube). A schematic of a tube-transducer arrangement is presented in Figure 2 (a), next to a schematic of the experimental setup used for the evaluation of dynamic effects in Wells turbines (Figure 2 (b) [4, 7, 8]. The similarity between the two systems is evident.

When measuring a dynamically changing pressure with the instrument

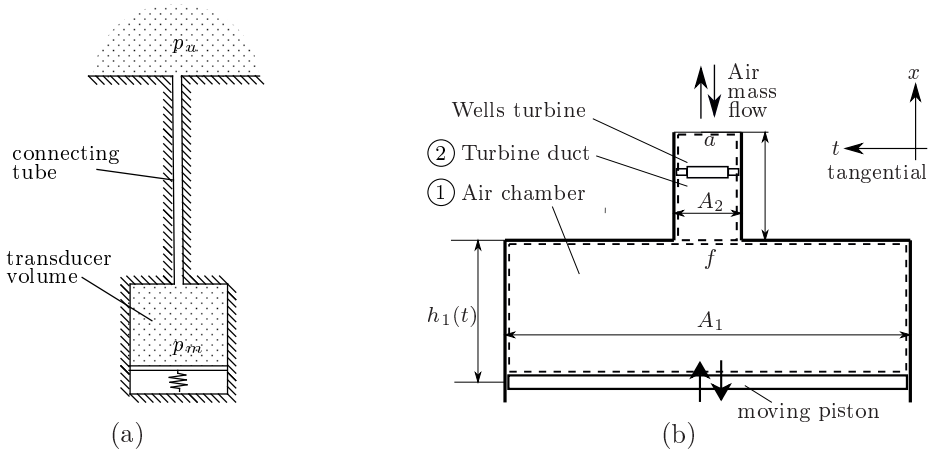

Figure 2: Schematics of tube-transducer system (left) and laboratory OWC system (right) used in [4]

in Figure 2 (a), attention needs to be payed to the delay that can exist between flow conditions just outside the duct (the pressure one seeks to know, p_u) and inside the volume (the pressure that is actually measured by the transducer, p_m). This is explained in detail in [61, Chapter 6.6: Dynamic Effects of Volumes and Connecting Tubing], where an LPM approach is used to evaluate the phase difference between measured and actual pressures. An adaptation of this approach will be presented in this work.

This approach will allow to derive a ordinary differential equation linking the piston-based flow coefficient ϕ_p and a local flow coefficient ϕ_l. The former was used in [4] to represent the turbine's operating point, assuming no compressibility in the chamber and therefore no delay between piston velocity and mass-flow through the duct. The latter, calculated using the actual value of flow velocity inside the duct, was used in the experiments from Paderi and Puddu [8, 9], and in the CFD simulations from Ghisu *et al.* [49, 50, 51].

$$\phi_p = \frac{V_p}{\omega r_m}\frac{A_1}{A_2}; \quad \phi_l = \frac{V_2}{\omega r_m} \tag{2}$$

where V_p is the piston speed, V_2 is the flow velocity inside the turbine duct, r_m is the turbine mean radius, and A_1 and A_2 are the cross-sections of air chamber and turbine, respectively.

The LPM model of the OWC-Wells turbine system can be derived by

applying the laws of conservation of mass and axial momentum to the variable air volume in the chamber (① in Figure 1) and to the turbine duct (②), respectively.

$$\begin{cases} \dfrac{\mathrm{d}M_1}{\mathrm{d}t} = h_1 A_1 \dfrac{\mathrm{d}\rho_1}{\mathrm{d}t} + \rho_1 A_1 \dfrac{\mathrm{d}h_1}{\mathrm{d}t} = -\rho_f V_2 A_2 & \text{(3a)} \\ \dfrac{\mathrm{d}(\rho_2 V_2 A_2 L)}{\mathrm{d}t} = (p_1 - p_a) A_2 + F_x & \text{(3b)} \end{cases}$$

In the above equation, M_1 is the mass of air in the chamber, h_1 and is the chamber's (variable) height, L is the turbine's duct cross-section length, ρ and p are the fluid's density and pressure. Subscript 1 and 2 refer to air chamber and turbine duct, respectively, f refers to the interface between volumes ① and ②, and a to the duct exit (to the ambient). F_x is the axial force that the turbine exerts on the fluid inside the turbine duct. The value assigned to ρ_f is fundamental to determine the mass-flow leaving or entering the air chamber:

$$\rho_f = \begin{cases} \rho_1 & \text{if } V_2 \geq 0 \\ \rho_2 & \text{if } V_2 < 0 \end{cases} \tag{4}$$

It should be noted that when deriving the approximated equation for the conservation of axial-momentum in the duct (equation (3b)), a few assumptions have been made:

- Viscous forces on the turbine duct's walls have been neglected, since they are usually significantly smaller than the turbine axial aerodynamic force F_x
- Compressibility of air within the turbine duct (but not in the air chamber) has been neglected. This means that ρ_2 is assumed equal to ρ_a, and that the difference between the axial momentum fluxes entering and leaving the volume is neglected
- The left-hand side of the axial momentum equation (equation (3b)) represents an approximation for the inertial force acting on the mass of air contained in the duct. For the approximation to be strictly valid, the average of $\rho_2 V_{x,2}$ in the turbine duct must be equal to the product of the averages of the two quantities ($\overline{\rho_2 V_{x,2}} = \overline{\rho_2}\,\overline{V_{x,2}}$). The error produced with this approximation has been evaluated for the CFD simulations

reported in [50, 62] and was never above 0.1%. A comparison of the two quantities for different values of the flow coefficient is reported in Figure 3.

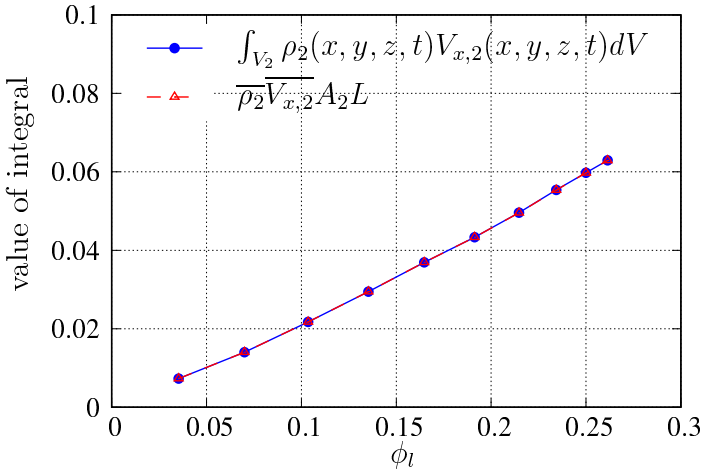

Figure 3: Approximation of the axial momentum in the turbine duct (from [50])

Equations (3a) and (3b) lead to 2 important considerations. From equation (3a), a delay between the velocity of the piston and the velocity of the airflow in the turbine duct exists, caused by the compressibility of air in the air chamber, and proportional to the ratio of chamber to duct dimensions. This phenomenon is well-documented in existing OWC analyses [26, 27, 28, 30]. From equation (3b), a delay also exists between the pressure drop in the turbine duct and the aerodynamic axial force acting on the turbine. This delay is needed to accelerate the mass of air within the turbine duct, and it is proportional to the volume of the duct. A difference between the relative chamber pressure during acceleration and deceleration phases should not be confused for an aerodynamic hysteresis, which should be evaluated on F_x or by measuring the pressure drop between two sections as close as possible to the turbine [8, 9]. The delay between pressure drop and turbine forces is often neglected in the analysis of OWC systems [26, 27, 28, 59, 29, 30]: with this further assumption, equation (3b) becomes a simple algebraic equation and the delay between piston movement and pressure drop can be modeled with a first-order ordinary differential equation. In this work, the inertial term in equation (3b) is maintained for completeness, also in consideration

that it was often found to be non-negligible in CFD analyses [50], although smaller than the delay deriving from equation (3a).

Wells turbine performance is represented in terms of non-dimensional coefficients of pressure drop p^* and torque T^*, as a function of flow coefficient ϕ_p, which in the experiment of Setoguchi [4] is calculated based on piston speed $V_p = -dh_1/dt$.

$$p^* = \frac{p_1 - p_a}{\rho_f \omega^2 {r_m}^2}; \quad T^* = \frac{T}{\rho_f \omega^2 {r_m}^5}; \tag{5}$$

where ρ_f is the flow density upstream of the turbine (inside the chamber or outside the duct during outflow and inflow, respectively, as in equation (4). The definitions used in [4] for the non-dimensional performance parameters have been modified to follow the rules of dimensional analysis [30].

The equations in (3) can be written in terms of the non-dimensional coefficients in (5), by dividing the mass conservation equation by $(\rho_a \omega r_m A_2)$ and the momentum equation by $(\rho_f (\omega r_m)^2 A_2)$:

$$\begin{cases} \dfrac{h_1}{r_m}\dfrac{A_1}{A_2}\dfrac{\mathrm{d}(\rho_1/\rho_a)}{\mathrm{d}(t\omega)} + \dfrac{\rho_1}{\rho_a}\dfrac{A_1}{A_2}\dfrac{\mathrm{d}(h_1/r_m)}{\mathrm{d}(t\omega)} = -\dfrac{\rho_f}{\rho_a}\dfrac{V_2}{\omega r_m} \\ \dfrac{\rho_a}{\rho_f}\dfrac{L}{r_m}\dfrac{\mathrm{d}(V_2/(\omega r_m))}{\mathrm{d}(t\omega)} = \dfrac{(p_1 - p_a)}{\rho_f (\omega r_m)^2} + \dfrac{F_x}{\rho_f (\omega r_m)^2 A_2} \end{cases} \tag{6}$$

Assuming compression and expansion processes inside the OWC chamber to be isentropic, as in [27, 28, 30], and introducing the following non-dimensional parameters:

$$\frac{A_1}{A_2}\frac{\mathrm{d}(h_1/r_m)}{\mathrm{d}(t\omega)} = -\phi_p \qquad \frac{V_2}{\omega r_m} = \phi_l \qquad \frac{p_1 - p_a}{\rho_f (\omega r_m)^2} = p^*$$

$$\frac{\rho_1}{\rho_a} = \rho^* = \frac{(\omega r_m)^2}{a^2} p^* + 1 \qquad \frac{F_x}{\rho_f (\omega r_m)^2 A_2} = c_x \qquad t\,\Omega = \frac{t\omega}{\omega/\Omega} = t^*$$

equation (6) becomes:

$$\begin{cases} \dfrac{h_1 A_1 \Omega}{A_2}\dfrac{(\omega r_m)}{a^2}\dfrac{\mathrm{d}p^*}{\mathrm{d}t^*} - \left(\dfrac{(\omega r_m)^2}{a^2} p^* + 1\right)\phi_p = -\dfrac{\rho_f}{\rho_a}\phi_l \\ \dfrac{\rho_a}{\rho_f}\dfrac{L}{r_m}\dfrac{\Omega}{\omega}\dfrac{\mathrm{d}\phi_l}{\mathrm{d}t^*} = p^* + c_x \end{cases} \tag{7}$$

where c_x a non-dimensional coefficient for the aerodynamic axial turbine force, Ω the piston angular frequency, a the local speed of sound, calculated

using the local temperature ($a^2 = \gamma RT$), and t^* a non-dimensional time. Equation (7) represents a system of two first-order non-linear ordinary differential equations with p^* and ϕ_l representing the unknowns and ϕ_p the external forcing. c_x needs to be provided as a function of other working parameters. It should be noted that the delay between p^* and c_x is often neglected in OWC analyses [26, 27, 28, 59, 29, 30]. In the same works, the axial force coefficient p^* is assumed to be a linear function of ϕ_l, for a Wells turbine. In this work, a similar relation will be used between c_x and ϕ_l, while p^* will be calculated through equation (7).

Given the experimental results from Puddu *et al.* [8, 9], the CFD results from Ghisu *et al.* [49, 50, 51, 54], and the literature survey presented in Section 2, the assumption of a negligible turbine aerodynamic hysteresis appears justified. The force coefficient c_x can therefore be considered a function of only the local flow coefficient ϕ_l. It should be emphasized that the validity of this hypothesis will be verified by comparing the results of the LPM model with the experimental data of [4] and with the authors' previous CFD analyses [50], in Section 4. With these assumptions, differentiating the momentum equation and replacing dp^*/dt^* from the continuity equation, equation (7) can be converted to a single second order differential equation:

$$\frac{\rho_a}{\rho_f}\frac{L}{r_m}\frac{\Omega}{\omega}\frac{\mathrm{d}^2\phi_l}{\mathrm{d}t^{*2}} + \frac{L}{r_m}\frac{\Omega}{\omega}\frac{\mathrm{d}}{\mathrm{d}t^*}\left(\frac{\rho_a}{\rho_f}\frac{\mathrm{d}\phi_l}{\mathrm{d}t^*} + \frac{\mathrm{d}c_x}{\mathrm{d}t^*} + \frac{a^2}{(\omega r_m)(h_1\Omega)}\frac{A_2}{A_1}\frac{\rho_f}{\rho_a}\phi_l\right) = \frac{a^2}{(\omega r_m)(h_1\Omega)}\frac{A_2}{A_1}\left(1 + \frac{(\omega r_m)^2}{a^2}p^*\right)\phi_p \tag{8}$$

It should be noted that the second-order ordinary differential equation (8) reverts to a first-order equation if inertial effects in the turbine duct are neglected, as in [26, 27, 28, 59, 29, 30].

Due to the non linearities, equation (8) must either be solved numerically, and the results will be shown in Section 4, or analytically after linearization. The latter has the advantage of allowing a rapid analysis of the relative importance of the different parameters appearing in equation (8), and can be done by assuming:

$$h_1 \approx h_{10} \qquad\qquad \left(1 + \frac{(\omega r_m)^2}{a^2}p^*\right) \approx 1$$

$$\frac{\rho_f}{\rho_a} \approx 1 \qquad\qquad a \approx a_0 \quad c_x = c_{x,\phi}\phi_l \tag{9}$$

awhere a_0 is the reference speed of sound (calculated with the ambient temperature). It should be noted that the last assumption in equation (9) entails a linear dependence between ϕ_l and c_x. This is justified by the results in [50] (reported in Appendix B), and a similar assumption has often been used in OWC analyses to represent the turbine's characteristics [26, 27, 29, 30]. The impact of all these assumptions will be verified in Section 4, where analytical and numerical (without the assumptions in equation (9)) solutions of equation (8) will be presented. The parameter $c_{x,\phi}$ (the slope of the c_x-ϕ_l curve, derived by fitting CFD analyses for the same problem [50], reported in Appendix B) represents a measure of the turbine damping on the OWC system.

After linearization, equation (8) becomes:

$$\underbrace{\frac{L}{r_m}\frac{\Omega}{\omega}}_{A}\frac{\mathrm{d}^2\phi_l}{\mathrm{d}t^{*2}} + \underbrace{c_{x,\phi}}_{B}\frac{\mathrm{d}\phi_l}{\mathrm{d}t^*} + \underbrace{\frac{a_0^2}{(\omega r_m)(h_{10}\Omega)}\frac{A_2}{A_1}}_{C}\phi_l = \underbrace{\frac{a_0^2}{(\omega r_m)(h_{10}\Omega)}\frac{A_2}{A_1}}_{D}\phi_p \tag{10}$$

The solution to equation (10) can be seen in terms of its transfer function $G(\Omega/\Omega_n)$:

$$\begin{aligned} G\left(\frac{\Omega}{\Omega_n}\right) &= \frac{\phi_l}{\phi_p} = \frac{D}{-A + Bj + C} = \frac{\dfrac{D}{C}}{-\dfrac{A}{C} + \dfrac{B}{C}j + 1} = \\ &= \frac{\dfrac{D}{C}}{-\left(\dfrac{\Omega}{\Omega_n}\right)^2 + 1 + 2\zeta\left(\dfrac{\Omega}{\Omega_n}\right)j} \end{aligned} \tag{11}$$

In the above equations, Ω_n is the natural angular frequency and ζ the damping ratio of the system:

$$\Omega_n = \sqrt{\frac{C}{A}}\Omega = a_0\sqrt{\frac{1}{h_{10}L}\frac{A_2}{A_1}} \tag{12}$$

$$2\zeta = \frac{B}{C}\frac{\Omega_n}{\Omega} = \frac{B}{C}\sqrt{\frac{C}{A}} = \frac{B}{\sqrt{AC}} = \frac{c_{x,\phi}}{\sqrt{\dfrac{L}{h_{10}}\dfrac{A_2}{A_1}\dfrac{a_0^2}{\omega r_m}}} \tag{13}$$

The solution to equation (10) is therefore:

$$\phi_l = \phi_{l0}\, e^{jt^* + \xi_{owc,0}} \tag{14}$$

where:

$$\phi_{l0} = |\phi_l| = |\phi_p| \left| G\left(\frac{\Omega}{\Omega_n}\right) \right| \tag{15}$$

$$\phi_p = \phi_{p0}\, e^{jt^*} \tag{16}$$

$$\tag{17}$$

$$\begin{aligned} \left| G\left(\frac{\Omega}{\Omega_n}\right) \right| &= \frac{\dfrac{D}{C}}{\sqrt{\left[\left(-\dfrac{\Omega}{\Omega_n}\right)^2 + 1\right]^2 + \left[2\zeta\left(\dfrac{\Omega}{\Omega_n}\right)\right]^2}} \\ &= \frac{D}{\sqrt{(C-A)^2 + B^2}} \end{aligned} \tag{18}$$

$$\begin{aligned} \xi_{owc,0} &= \tan^{-1}\left(\frac{-2\zeta \dfrac{\Omega}{\Omega_n}}{-\left(\dfrac{\Omega}{\Omega_n}\right)^2 + 1} \right) = \tan^{-1}\left(\frac{-B}{C-A}\right) \\ &= \tan^{-1}\left(\frac{c_{x,\phi}}{\dfrac{L}{r_m}\dfrac{\Omega}{\omega} - \dfrac{a_0^2}{(\omega r_m)(h_{10}\Omega)}\dfrac{A_2}{A_1}} \right) \end{aligned} \tag{19}$$

Equation (19) is the fundamental result of this section, and deserves some attention. Because of the damping produced by the first order term in equation (10) (the resistance produced by the turbine), a delay $\xi_{owc,0}$ exists between piston movement and mass-flow passing in the turbine duct. It will be shown how this *OWC hysteresis*, already discussed by [26, 27, 28, 30] among others, is by far the largest contribution to the hysteresis measured in the experiments of [1, 2, 3, 4, 5] and should not have been ignored when discussing turbine performance.

The LPM (equation (8)) has also been solved numerically, without the assumptions introduced in equation (9), by integrating in time, with a semi-implicit time-marching scheme. The value of the force coefficient c_x has been obtained as a function of the local flow coefficient ϕ_l, by interpolating the values available from the CFD simulations [50] (the data used are reported in Appendix B). The comparison of analytical and numerical solutions will give also the opportunity to quantify the impact of the assumptions in equation (9). Attention will be placed in the choice of the time step, in order to avoid the introduction of spurious phase delays, similar to the ones introduced in [11, 10, 12, 13, 14, 15, 16, 17, 23] and others.

4. Results

The model introduced in Section 3 has been applied to 3 experimental analyses presented in [4]. The only parameter differentiating these experiments is the turbine solidity σ, that has a direct effect on the turbine axial-force coefficient $c_{x,\phi}$, and thus on the damping of the system in equations (8) and (10). Geometrical dimensions and operating conditions are reported in Table 1. For all 3 experiments, the operating non-dimensional frequency is 1.2×10^{-3}. Dimensions and operating conditions have been extracted from [4], apart from the chamber height, derived from [63]. The value of piston stroke has been set to obtain the required range of turbine flow coefficients observed in the experiments. The same values were also used for the unsteady CFD simulations of [50].

With these data, using the equations provided by [46], a value of 0.0036 can be estimated for the turbine aerodynamic phase delay, independent from the turbine solidity. Equation (19) allows the evaluation of the phase difference due to the OWC-turbine system dynamics, resulting in values ranging from 0.0306 for $\sigma = 0.48$, to 0.0843 for $\sigma = 0.67$.

From these results, it is clear that the contribution to phase delay, or hysteresis, given by turbine aerodynamics is at least one order of magnitude smaller than the contribution given by the compressibility of air within the OWC chamber.

Figure 4 compares the results obtained with both the analytical and a numerical solution of equation (7), using a semi-implicit time-marching scheme and a time-step of 5×10^{-4} s, with the experimental results of [4], and with the CFD analysis of [50]. A verification of the appropriateness of the value used for the temporal discretization will be given in Appendix A. The problem has

Table 1: Geometrical and operating data for Setoguchi's experiments [4]

Experiment	1	2	3
chamber diameter [m]		1.4 m	
chamber height [m]		1.2 m	
piston stroke [m]		0.423 m	
rotor tip diameter [mm]		300 mm	
rotor hub diameter [mm]		210 mm	
tip clearance [mm]		1 mm	
chord length c [mm]		90 mm	
sweep ratio [-]		0.417	
number of blades [-]	5	6	7
blade profile [-]		NACA0020	
solidity at tip radius σ [-]	0.48	0.57	0.67
$c_{x,\phi}[-]$	2.05	3.11	5.67
rotational speed [rpm]		2500 rpm	
piston frequency f [s^{-1}]		6 s	
Reynolds number Re [-]		2×10^5	
Mach number M [-]		0.1	
turbine non-dimensional frequency k [-]		0.0012	
coefficient A in equation (10) [-]		0.01569	
coefficient B in equation (10) [-]	2.046	3.106	5.673
coefficient $C = D$ in equation (10) [-]		57.68	
phase delay due to turbine $\lvert\xi_a\rvert$ [1] [-]		0.0036	
phase delay due to OWC $\lvert\xi_{owc,0}\rvert$ [-]	0.0306	0.0464	0.0843

been solved for 4 piston periods, in order to obtain a periodically stable solution. Plots of non-dimensional pressure drop p^* and torque T^*, as a function of the flow coefficient based on piston speed ϕ_p, for the different turbine solidities, are shown in Figure 4. The LPM approach (without any account for aerodynamic turbine hysteresis) is able to predict with remarkable accuracy the hysteretic loop found in the experiments, and it approximates the CFD results even more closely, confirming that a computationally expensive CFD solution is not needed to study the hysteresis in OWC-turbine systems. The turbine solidity has a direct effect on the slope of the c_x vs. ϕ_l curve, i.e. on the damping term in equation (8), and hence on the width of the hysteretic loop, as predicted in equation (19). The agreement between analytical (af-

ter linearization) and numerical solutions is excellent, demonstrating that the impact of the assumptions made to linearize the LPM (equation (9)) is minimal.

The cause of the hysteresis shown in Figure 4 and present in the experiments of [4] can be deduced in Figure 5, where the temporal evaluations of piston and local flow coefficients are shown, using analytical and numerical LPM, in comparison with the CFD results from [50]. The agreement is remarkable, showing that the OWC-turbine interaction can be described as a second order damped system, driven by the movement of the piston. The compressibility of air in the OWC chamber generates a delay between piston movement and flow in the duct, that is sufficient by itself to explain all the hysteresis found in the experiments [4]. The delay increases for larger values of the turbine damping, as shown in Figure 5, and as predicted by equation (19).

These results are corroborated by the experimental analyses of [8, 9], and the CFD results of [49, 50, 51, 54], where hysteresis was only present if performance was presented as a function of the conditions inside the chamber and not in the vicinity of the turbine. Had this simple analysis been performed earlier, it could have guided experimental and numerical research, probably avoiding the errors made in several scientific works. It should also be noted that the presence of a delay between water level displacement and turbine mass-flow is often discussed in OWC system analyses [26, 27, 28, 59, 29, 30], frequently ignored in turbine analyses under unsteady operating conditions [1, 2, 3, 4, 10, 23].

It should be noted that, at least for the system under examination, $C >> A$. This confirms the assumption often made in wave-to-wire models of ($p^* \simeq c_x$) [26, 27, 28, 59, 29, 30]. The phase difference is therefore approximately equal to:

$$\xi_{owc,0} \simeq \tan^{-1}\left[-c_{x,\phi}\frac{\omega r_m}{a_0}\frac{\Omega L}{a_0}\frac{A_1 h_{10}}{A_2 L}\right] \tag{20}$$

Equation (20) shows how the OWC hysteresis is linearly dependent on several non-dimensional parameters.

- The turbine axial force coefficient $c_{x,\phi}$
- The non-dimensional blade speed $\omega r_m/a_0$
- The non-dimensional piston frequency $\Omega L/a_0$

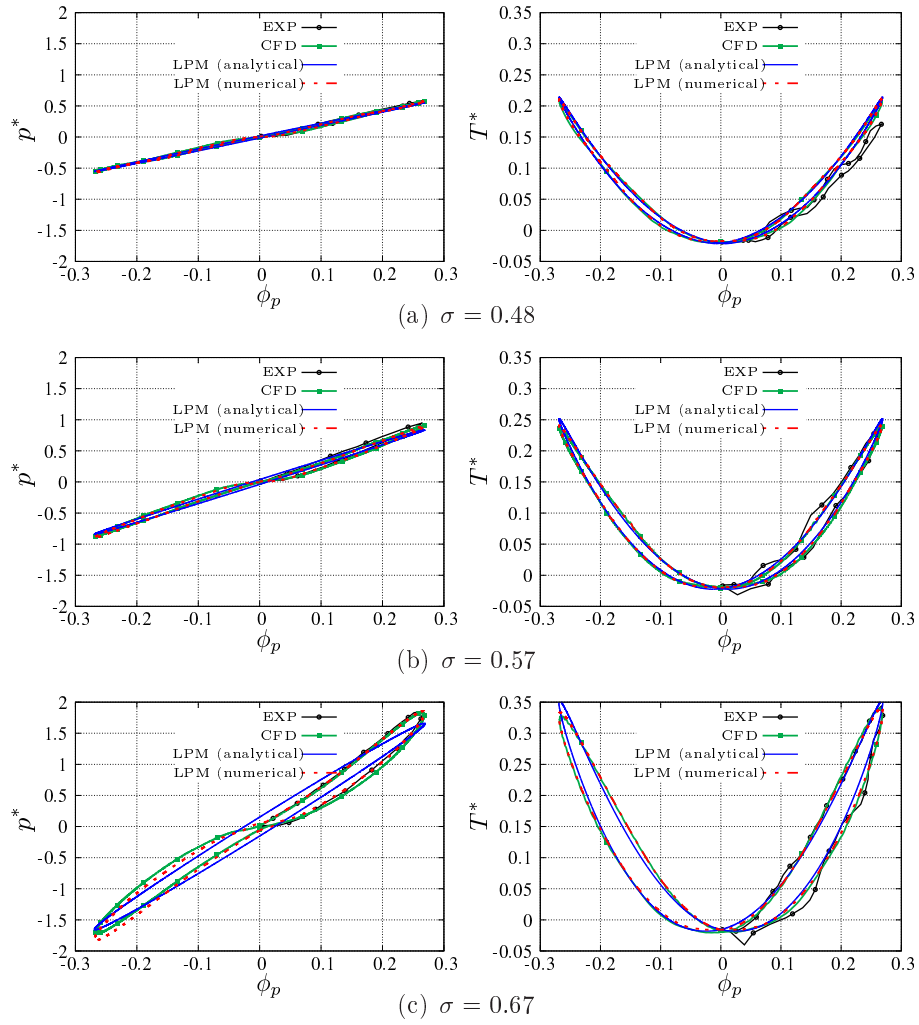

Figure 4: Comparison of LPM results with experimental data from [4], for different turbine solidities

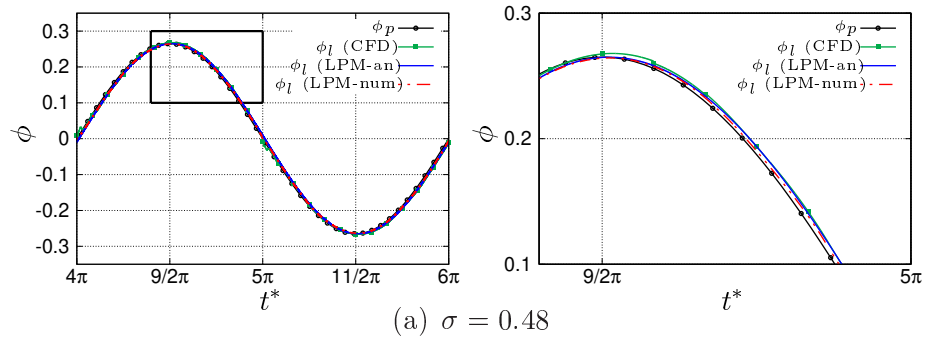

(a) $\sigma = 0.48$

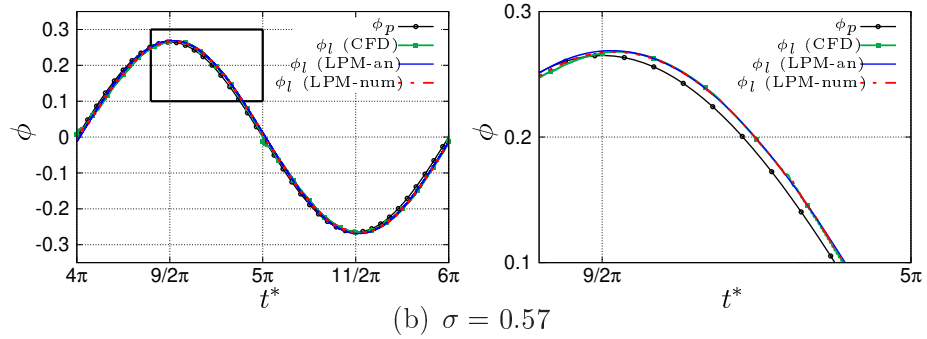

(b) $\sigma = 0.57$

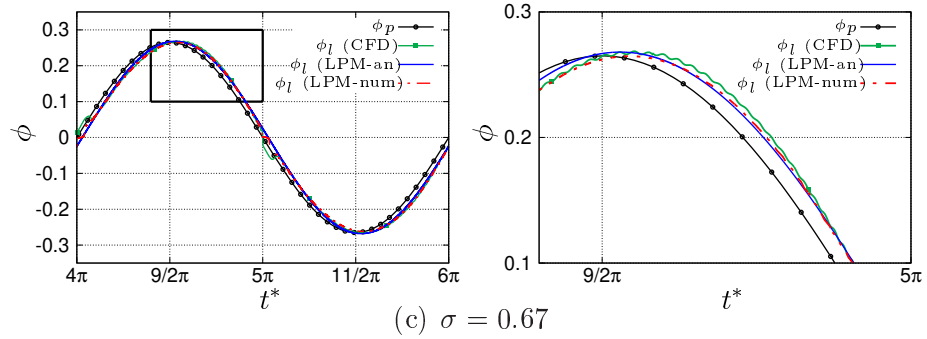

(c) $\sigma = 0.67$

Figure 5: Temporal evolution of piston and local flow coefficients, for different turbine solidities

- The ratio of chamber to turbine duct volumes $A_1 h_{10}/A_2 L$

In Table 1 and Figure 4, it was shown how increasing the turbine solidity (and hence $c_{x,\phi}$) produces an increase in the OWC hysteresis. The same would be true for any of the parameters introduced in equation (20). Typically, non-dimensional blade speed and piston frequency are significantly larger for full-scale OWC systems, where an even larger OWC hysteresis can be expected [64, 65, 66]. The value of the OWC hysteresis needs to be quantified accurately when using a control strategy to maximize the energy collected by the system, as in [67, 68, 69, 70, 71].

Differences in performance for OWC-installed turbines have been observed not only between acceleration and deceleration phases, but also between *outflow* and *inflow* phases (also referred to with the terms *exhalation* and *inhalation*). These are also discussed in detail in [8, 9] (experiments) and [49, 50, 51, 54] (CFD), and are due to the geometrical differences between the two sides of the turbine (duct and chamber) and to the difference between flow conditions in the atmosphere and inside the air chamber (larger turbulence and presence of swirl deriving from the previous phase). Most of these cannot be accounted for with the current LPM. The different geometry (decreasing vs. increasing chamber volume) is accounted, as it can be seen in equation (7), and in Figure 4, where the inflow loop is slightly less pronounced. The same difference can also be found in [8, 9, 51, 54].

4.1. Simulating the presence of an (unlikely) aerodynamic hysteresis with the lumped parameter model

The LPM, as it was presented in the previous section, proves that the hypothesis of a negligible hysteresis is perfectly valid, as the experimental data of [4] can be fully explained with the presence of only a volume hysteresis caused by the compressibility of air inside the OWC chamber.

The absence of aerodynamic hysteresis in the turbine has been already proved by means of experimental [8, 9] and numerical (CFD) analyses [49, 50, 51, 54]. This section shows how a similar conclusion could have been reached with the LPM introduced in Section 3, with minor modifications.

Rather than assuming a negligible aerodynamic hysteresis (i.e. $c_x = c_{x,\phi}\phi_l$), one could assume the presence of a yet to be determined aerodynamic hysteresis. In complex notation, introducing the non-dimensional reactance f_a:

$$c_x = \frac{c_{x,\phi}}{\sqrt{1+f_a^2}}(1+f_a j)\phi_l \tag{21}$$

f_a needs to be negative for the aerodynamic forces to lag behind the local flow coefficient ϕ_l, therefore producing an anti-clockwise hysteretic loop. The phase difference ξ_a between c_x and ϕ_l, that represents the aerodynamic hysteresis, can be calculated as follows:

$$\xi_a = \tan^{-1}(f_a) \tag{22}$$

With this assumption, equation (10) becomes:

$$\frac{L}{r_m}\frac{\Omega}{\omega}\frac{\mathrm{d}^2\phi_l}{\mathrm{d}t^{*2}} + \frac{c_{x,\phi}}{\sqrt{1+f_a^2}}(1+f_a j)\frac{\mathrm{d}\phi_l}{\mathrm{d}t^*} + \frac{a_0^2}{(\omega r_m)(h_{10}\Omega)}\frac{A_2}{A_1}\phi_l = \frac{a_0^2}{(\omega r_m)(h_{10}\Omega)}\frac{A_2}{A_1}\phi_p \tag{23}$$

or equivalently:

$$A\frac{\mathrm{d}^2\phi_l}{\mathrm{d}t^{*2}} + \frac{B}{\sqrt{1+f_a^2}}(1+f_a j)\frac{\mathrm{d}\phi_l}{\mathrm{d}t^*} + C\phi_l = D\phi_p \tag{24}$$

where A, B, C, and D are the coefficients in equation (10), obtained when assuming $\xi_a = 0$. For this system, the transfer function can be written as:

$$G = \frac{D}{C - A - \dfrac{Bf_a}{\sqrt{1+f_a^2}} + \dfrac{B}{\sqrt{1+f_a^2}}j} \tag{25}$$

and the OWC phase (i.e. the difference in phase between ϕ_l and ϕ_p caused by the OWC geometry) can therefore be calculated as:

$$\xi_{owc} = \tan^{-1}\left(\frac{-\dfrac{B}{\sqrt{1+f_a^2}}}{C - A - \dfrac{Bf_a}{\sqrt{1+f_a^2}}}\right) \tag{26}$$

Note how the previous equation reduces to equation (19) if the assumption of a negligible aerodynamic hysteresis, i.e. $f_a = 0$, is introduced at this point. The total hysteresis, i.e. the hysteresis between piston motion and turbine forces, is the sum of OWC hysteresis and aerodynamic hysteresis:

$$\xi_{tot} = \xi_{owc} + \xi_a \tag{27}$$

In Section 4, in the absence of aerodynamic hysteresis, the LPM predicts an OWC hysteresis $\xi_{owc,0} = -0.0843$. Assuming now 3 values for the aerodynamic hysteresis (twice, equal, and one fourth of the value obtained in Section 4) for $\xi_{owc,0}$, the new OWC hysteresis, in the presence of a turbine aerodynamic hysteresis, can be determined from equations (26) and (27). The values obtained are presented in Table 2.

Table 2: Effect of assuming the presence of an aerodynamic hysteresis on the OWC hysteresis and on the total hysteresis of the system

$\xi_a/\xi_{owc,0}$	ξ_{owc}	ξ_{tot}
2	-0.0801	-0.2523
1	-0.0822	-0.1680
0.25	-0.0837	-0.1048
0	-0.0843	-0.0843

The presence of an aerodynamic hysteresis has little effect on the OWC hysteresis, but the total hysteresis (between turbine forces and piston movement) is clearly affected by its presence, since the two contributions act in the same direction, i.e. they produce a lag between flow conditions in the chamber and in the duct, and flow conditions in the duct and aerodynamic turbine forces, respectively. This is also shown graphically in Figure 6, that reports the turbine torque coefficient as a function of the piston-based flow coefficient, in the presence of different values for the aerodynamic hysteresis, for the highest solidity turbine ($\sigma = 0.67$). It is clear that the aerodynamic hysteresis needs to be smaller than the OWC hysteresis, for the model to match the experimental data.

To further prove this conclusion, in Figure 7, the root mean square error (difference between experimental data and numerical LPM results), is plotted for different values of the ratio between aerodynamic hysteresis and OWC hysteresis. The error is non-dimensionalized with the error produced assuming $\xi_a = 0$. Especially for the highest solidity case (the case with the largest total hysteresis), it is clear that the only acceptable explanation for the cause of the delay between piston movement and aerodynamic forces is the absence of a meaningful aerodynamic hysteresis. In other words, the aerodynamic hysteresis has to be significantly smaller than the OWC hysteresis. And this is exactly what the analysis presented in Table 1 had suggested.

The same is also true for the turbines with a lower solidity ($\sigma = 0.48$ and $\sigma = 0.57$), even though this is less evident in Figure 7 because of the lower

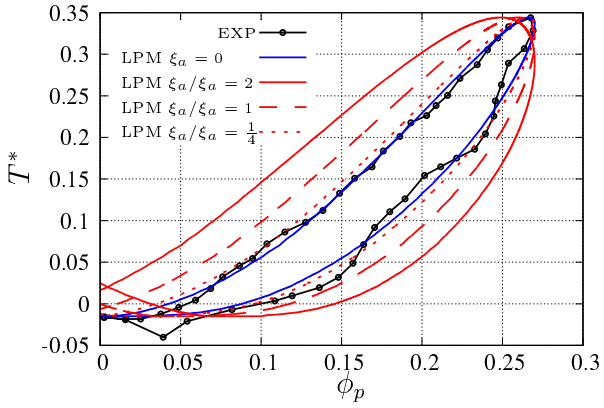

Figure 6: Effect of the presence of aerodynamic hysteresis on the global hysteresis (torque coefficient) for the highest solidity turbine ($\sigma = 0.67$)

absolute values of the hysteresis, that, especially for the $\sigma = 0.48$ case, becomes of the same order of magnitude of the oscillations in the experimental data.

These results are confirmed by experimental [8, 9] and CFD analyses [49, 50, 51, 54] conducted by the authors of this article, where the absence of a measurable aerodynamic hysteresis is evident.

It is important to underline the importance of this LPM analysis, because, had it been conducted in the past, it would have guided experimental and higher-fidelity numerical research into devising the right experimental setup to verify and quantify the presence of an (unlikely) aerodynamic hysteresis. It should also be noted that the presence of a delay between conditions inside the chamber and turbine mass-flow is often discussed in OWC models [26, 27, 28, 29, 30]. However, this information has been often ignored in Wells turbine analyses under unsteady operating conditions [1, 2, 3, 4, 10, 23].

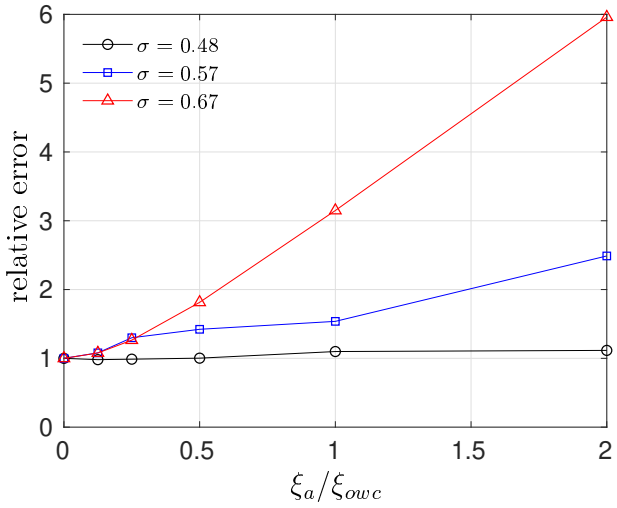

Figure 7: Root-mean-square error between numerical (LPM) results and experimental data

5. Conclusions

The presence of aerodynamic hysteresis in Wells turbines has been the subject of a large number of publications in the last decades. Its presence had been discovered in experimental analyses, which studied the turbine behavior in laboratory setups that used a mechanic piston inside a large cylinder to reproduce the periodic mass-flow through the rotor. The commonly accepted explanation was found using CFD simulations, that reproduced only part of the laboratory experiment, i.e. the turbine rotor, neglecting the importance of the large chamber used to reproduce the periodic operating conditions. This is even more surprising considering that the importance of compressibility effects inside the chamber is often discussed in OWC analyses [26, 27, 28, 29, 30].

This work suggests a re-examination of the origin of the alleged hysteresis using a lumped parameter model, based on 3 anomalies. First, during its operation, a Wells turbine experiences a continuous change in incidence angle, in a way that is not dissimilar to what happens to oscillating airfoils and wings, but at non-dimensional frequencies too low to generate any visible dynamic effects (i.e. hysteresis) in oscillating airfoils [34, 46]. Second, recent works have shown how the aerodynamic hysteresis reported in many CFD simulations was caused by numerical errors [49, 50, 51, 54]. Third, in

several experimental works [8, 9], the aerodynamic hysteresis was shown to be negligible.

This work shows how the real cause of the hysteresis, i.e. the delay between flow conditions in the chamber and in the turbine duct, could have been predicted with the simple lumped parameter model, which could have also guided other experimental and higher-fidelity numerical research, providing important directions on how to devise ad-hoc analyses to correctly measure the presence and extent of aerodynamic hysteresis.

It is also shown that the real cause of the hysteresis reported in several experimental works is the compressibility of air within the OWC chamber and that any aerodynamic hysteresis is likely to be at least one order of magnitude lower than the OWC hysteresis, hence negligible.

Given its simplicity, accuracy, and short running times, the LPM presented in its work could be an ideal candidate to be used to estimate the phase delay between conditions in the OWC chamber and in the turbine duct when implementing control strategies aimed at maximizing the energy captured by the OWC system [67, 68, 69, 70, 71], on its own or in combination with similar systems modeling the behavior of the water column within the OWC.

Appendix A

Numerical errors are always present in numerical simulation, and it is good practice to evaluate their extent and impact on the solution, before analyzing any results. Many academic societies have written ad-hoc policies. For instance, the ASME Journal of Fluids Engineering has published a "Editorial Policy Statement on the Control of Numerical Accuracy" [55] that highlights the importance of presenting results that are independent from the discretization used. This process takes the name of *verification* and has the objective of assessing the correctness of the numerical simulation of the governing equations. It is distinct and different from the *validation*, which determines how appropriate the chosen model is in representing the reality, and is usually accomplished by comparing the numerical results with experimental data. It is important to highlight how unambiguous validation can be achieved only once discretization and iteration errors are isolated: only if computational uncertainties are negligible, then the uncertainties resulting from the conceptual model can be obtained through validation [72].

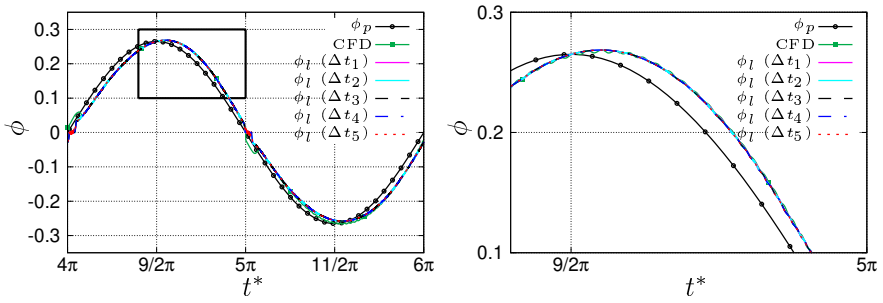

Figure 8: Verification of the temporal discretization on the estimation of the OWC hysteresis, using 3 time-step sizes

A careful verification of the numerical results is of fundamental importance in problem that deals with a hysteresis, i.e. a phase lag, as it is well known that an insufficient temporal discretization can lead to spurious phase errors, that can be confused with the problem under examination. An insufficient temporal discretization has been shown to cause a misinterpretation of the cause of the OWC-turbine hysteresis in many numerical (CFD) works [49, 50, 51, 54].

Figure 8 reports the effect of the temporal discretization on the evaluation of the temporal evolution of the local flow coefficient ϕ_l, obtained solving equation (8) with 5 different time-step sizes ($\Delta t_1 = 0.000125$ s, $\Delta t_2 = 0.00025$ s, $\Delta t_3 = 0.0005$ s, $\Delta t_4 = 0.001$ s and $\Delta t_5 = 0.002$ s). It is evident how no measurable difference exists among the 5 solutions, and therefore any of these time-step sizes can be used to evaluate the dynamic performance of the system. Above the last value tested, the numerical solution diverges, as the product of the Δt times the largest eigenvalue of the characteristic matrix of the system lies outside the stability region.

Appendix B

The LPM model developed in this work requires data for the turbine characteristics, i.e. the aerodynamic forces as a function of the operating conditions. In the CFD analysis from Ghisu *et al.* [50], it was shown how the turbine performance is a function only of the local flow coefficient ϕ_l. The data for the aerodynamic forces from [50], used to close the system in (7), are reported in Figure 9.

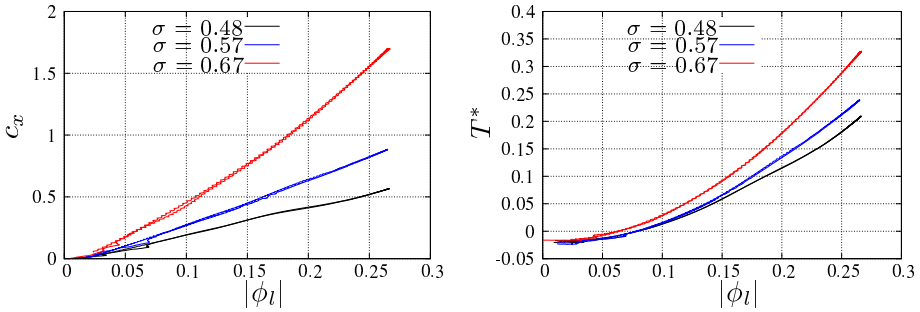

(a) Axial force coefficient (b) Torque coefficient

Figure 9: Turbine axial force and torque coefficients as a function of the local flow coefficient ϕ_l (from [50])

Acknowledgments

This work has been funded by the Regione Autonoma Sardegna under grant F72F16002880002 (L.R. 7/2007 n. 7 - year 2015).

References

[1] M. Inoue, K. Kaneko, T. Setoguchi, K. Shimamoto, Studies on Wells turbine for wave power generator(part 4: Starting and running characteristics in periodically oscillating flow), Bulletin of JSME 29 (250) (1986) 1177–82. doi:10.1248/cpb.37.3229.

[2] S. Raghunathan, T. Setoguchi, K. Kaneko, Hysteresis on Wells turbine blades, in: ASME Fluids Engineering Conference, no. 87-FE3, Cincinnati, USA, 1987.

[3] K. Kaneko, T. Setoguchi, H. Hamakawa, M. Inoue, Biplane axial turbine for wave power generator, International Journal of Offshore and Polar Engineering 1 (2) (1991) 122–128.

[4] T. Setoguchi, M. Takao, K. Kaneko, Hysteresis on Wells turbine characteristics in reciprocating flow, International Journal of Rotating Machinery 4 (1) (1998) 17–24.

[5] A. Thakker, R. Abdulhadi, The performance of Wells turbine under bi-directional airflow, Renewable Energy 33 (11) (2008) 2467–2474.

[6] B. S. Hyun, J. S. Suh, P. M. Lee, Investigation on the aerodynamic performance of a Wells turbine for ocean wave energy absorption, in: Transactions of the Society of Naval Architects of Korea, 1993.

[7] S. Camporeale, P. Filianoti, Behaviour of a small Wells turbine under randomly varying oscillating flow, in: Proceedings of the 8th European Wave and Tidal Energy Conference, Uppsala, Sweden, 2009, pp. 690–696.

[8] M. Paderi, P. Puddu, Experimental investigation in a Wells turbine under bi-directional flow, Renewable Energy 57 (2013) 570–576. doi:10.1016/j.renene.2013.02.016.

[9] P. Puddu, M. Paderi, C. Manca, Aerodynamic characterization of a Wells turbine under bi-directional airflow, Energy Procedia 45 (2014) 278–287. doi:10.1016/j.egypro.2014.01.030.

[10] Y. Kinoue, T. Setoguchi, T. H. Kim, K. Kaneko, M. Inoue, Mechanism of hysteretic characteristics of Wells turbine for wave power conversion, Journal of Fluids Engineering 125 (2) (2003) 302–307. doi:10.1115/1.1538629.

[11] T. H. Kim, T. Setoguchi, M. Takao, K. Kaneko, S. Santhakumar, Study of turbine with self-pitch-controlled blades for wave energy conversion, International Journal of Thermal Sciences 41 (1) (2002) 101–107. doi:10.1016/S1290-0729(01)01308-4.

[12] T. Setoguchi, Y. Kinoue, T. Kim, K. Kaneko, M. Inoue, Hysteretic characteristics of wells turbine for wave power conversion, Renewable Energy 28 (13) (2003) 2113–2127. doi:10.1016/S0960-1481(03)00079-X.

[13] Y. Kinoue, T. H. Kim, T. Setoguchi, M. Mohammad, K. Kaneko, M. Inoue, Hysteretic characteristics of monoplane and biplane Wells turbine for wave power conversion, Energy Conversion and Management 45 (9-10) (2004) 1617–1629.

[14] Y. Kinoue, T. Setoguchi, T. Kim, M. Mamun, K. Kaneko, M. Inoue, Hysteretic characteristics of the Wells turbine in a deep stall condition, Proceedings of the Institution of Mechanical Engineers Part M: Journal of Engineering for the Maritime Environment 218 (3) (2004) 167–173. doi:10.1243/1475090041737967.

[15] M. Mamun, Y. Kinoue, T. Setoguchi, T. Kim, K. Kaneko, M. Inoue, Hysteretic flow characteristics of biplane Wells turbine, Ocean Engineering 31 (11-12) (2004) 1423–1435. doi:10.1016/j.oceaneng.2004.03.002.

[16] M. Mamun, T. Setoguchi, Y. Kinoue, K. Kaneko, Visualization of unsteady flow phenomena of Wells turbine during hysteresis study, Journal of Flow Visualization and Image Processing 12 (2) (2005) 111–123. doi:10.1615/JFlowVisImageProc.v12.i2.20.

[17] Y. Kinoue, M. Mamun, T. Setoguchi, K. Kaneko, Hysteretic characteristics of Wells turbine for wave power conversion (effects of solidity and setting angle), International Journal of Sustainable Energy 26 (1) (2007) 51–60. doi:10.1080/14786450701359117.

[18] A. S. Shehata, K. M. Saqr, Q. Xiao, M. F. Shehadeh, A. Day, Performance analysis of Wells turbine blades using the entropy generation minimization method, Renewable Energy 86 (2016) 1123–1133. doi:10.1016/j.renene.2015.09.045.

[19] A. S. Shehata, Q. Xiao, M. El-Shaib, A. Sharara, D. Alexander, Comparative analysis of different wave turbine designs based on conditions relevant to northern coast of Egypt, Energy 120 (2017) 450–467. doi:10.1016/j.energy.2016.11.091.

[20] A. S. Shehata, Q. Xiao, K. M. Saqr, D. Naguib, A.and Alexander, Passive flow control for aerodynamic performance enhancement of airfoil with its application in Wells turbine – Under oscillating flow condition, Ocean Engineering 136 (2017) 31–53. doi:10.1016/j.oceaneng.2017.03.010.

[21] A. S. Shehata, Q. Xiao, M. M. Selim, A. H. Elbatran, D. Alexander, Enhancement of performance of wave turbine during stall using passive flow control: First and second law analysis, Renewable Energy 113 (2017) 369–392. doi:10.1016/j.renene.2017.06.008.

[22] A. Shehata, Q. Xiao, M. Kotb, M. Selim, A. Elbatran, D. Alexander, Effect of passive flow control on the aerodynamic performance, entropy generation and aeroacoustic noise of axial turbines for wave energy extractor, Ocean Engineering 157 (2018) 262–300. doi:10.1016/j.oceaneng.2018.03.053.

[23] Q. Hu, Y. Li, Unsteady RANS simulations of wells turbine under transient flow conditions, ASME Journal of Offshore Mechanics and Arctic Engineering 140(1). doi:10.1115/1.4037696.

[24] M. Penalba, J. Ringwood, A review of wave-to-wire models for wave energy converters, Energies 9 (7). doi:10.3390/en9070506.

[25] J. Kelly, W. Wright, W. Sheng, K. O Sullivan, Implementation and verification of a wave-to-wire model of an oscillating water column with impulse turbine, IEEE Transactions on Sustainable Energy 7 (2) (2016) 546–553. doi:10.1109/TSTE.2015.2504463.

[26] R. Jefferys, T. Whittaker, Latching Control of an Oscillating Water Column Device with Air Compressibility, Hydrodynamics of Ocean Wave-Energy Utilization (1986) 281–291doi:10.1007/978-3-642-82666-5-24.

[27] A. F. D. O. Falcão, P. A. P. Justino, OWC wave energy devices with air flow control, Ocean Engineering 26 (12) (1999) 1275–1295. doi:10.1016/S0029-8018(98)00075-4.

[28] P. Boccotti, Comparison between a U-OWC and a conventional OWC, Ocean Engineering 34 (5-6) (2007) 799–805. doi:10.1016/j.oceaneng.2006.04.005.

[29] G. Malara, F. Arena, Analytical modelling of an U-Oscillating Water Column and performance in random waves, Renewable Energy 60 (2013) 116–126. doi:10.1016/j.renene.2013.04.016.

[30] A. F. Falcão, J. C. Henriques, The spring-like air compressibility effect in oscillating-water-column wave energy converters: Review and analyses, Renewable and Sustainable Energy Reviews 112 (2019) 483–498. doi:10.1016/j.rser.2019.04.040.

[31] M. Kramer, Increase in the maximum lift of an airfoil due to a sudden increase in its effective angle of attack resulting from a gust, Tech. Rep. NASA Technical Memorandum 678, NASA (1932).

[32] J. G. Leishman, Dynamic stall experiments on the NACA 23012 aerofoil, Experiments in Fluids 9 (1-2) (1990) 49–58. doi:10.1007/BF00575335.

[33] J. M. Anderson, K. Streitlien, D. S. Barrett, M. S. Triantafyllou, Oscillating foils of high propulsive efficiency, Journal of Fluid Mechanics 360 (1998) 41–72. doi:10.1017/S0022112097008392.

[34] L. W. Carr, K. W. McAlister, W. J. McCroskey, Analysis of the development of dynamic stall based on oscillating airfoil experiments, Tech. Rep. NASA Technical Note D-8382, NASA (1977).

[35] K. W. McAlister, L. W. Carr, M. W. J., Dynamic stall experiements on the NACA 0012 airfoil, Tech. Rep. NASA Technical Paper 1100, NASA (1978). doi:10.1007/BF00575335.

[36] W. J. McCroskey, The phenomenon of dynamic stall, Tech. Rep. NASA Technical Memorandum 81264, NASA (1981). doi:10.1080/6008555886.

[37] K. W. McAlister, S. L. Pucci, W. McCroskey, L. W. Carr, An experimental study of dynamic stall on advanced airfoil sections. volume 2. pressure and force data, Tech. Rep. NASA Technical Memorandum 84245, NASA (1978).

[38] L. Y. Seto, R. A. M. Galbraith, The effect of pitch rate on the dynamic stall of the effect of pitch rate on the dynamic stall of a NACA 23012 aerofoil, in: Eleventh European Rotorcraft Forum, no. 34, London, United Kingdom, 1985.

[39] K. Kaufmann, C. Merz, A. Gardner, Dynamic stall simulations on a pitching finite wing, Journal of Aircraft 54 (4) (2017) 1303–1316. doi:10.2514/1.C034020.

[40] M. R. Visbal, D. J. Garmann, Analysis of dynamic stall on a pitching airfoil using high-fidelity large-eddy simulations, AIAA Journal 56 (1) (2017) 0–0. doi:10.2514/1.J056108.

[41] Y. J. Lee, K. B. Lua, Optimization of simple and complex pitching motions for flapping wings in hover, AIAA Journal 56 (6) (2018) 2466–2470. doi:10.2514/1.B34085.

[42] A. Medina, M. V. Ol, D. Greenblatt, H. Müller-Vahl, C. Strangfeld, High-amplitude surge of a pitching airfoil: Complementary wind- and water-tunnel measurements, AIAA Journal 56 (4) (2018) 1–7. doi:10.2514/1.J056408.

[43] S. Zeyghami, Q. Zhong, G. Liu, H. Dong, Passive pitching of a flapping wing in turning flight, AIAA Journal (2018) 1–9doi:10.2514/1.J056622.

[44] T. Van Buren, D. Floryan, A. J. Smits, Scaling and performance of simultaneously heaving and pitching foils, AIAA Journal (2018) 1–12arXiv:1801.07625, doi:10.2514/1.J056635.

[45] I. Gursul, D. J. Cleaver, Plunging oscillations of airfoils and wings: Progress, opportunities, and challenges, AIAA Journal (2018) 1–18doi:10.2514/1.J056655.

[46] L. E. Ericsson, J. P. Reding, Fluid mechanics of dynamic stall: Part 1 unsteady flow concepts, Journal of Fluids and Structures 2 (1988) 1–33. doi:10.1016/S0889-9746(88)80015-X.

[47] J. G. Leishman, Contributions to the experimental investigation and analysis of aerofoil dynamic stall, Ph.D. thesis, Department of Aeronautics and Fluid Mechanics, University of Glasgow (1984).

[48] T. Ghisu, P. Puddu, F. Cambuli, N. Mandas, P. Seshadri, G. T. Parks, Discussion on "Performance analysis of Wells turbine blades using the entropy generation minimization method" by Shehata, A. S., Saqr, K. M., Xiao, Q., Shahadeh, M. F. and Day, A., Renewable Energy 118 (2018) 386–392. doi:10.1016/j.renene.2017.10.107.

[49] T. Ghisu, P. Puddu, F. Cambuli, Numerical analysis of a Wells turbine at different non-dimensional piston frequencies, Journal of Thermal Science 24 (6) (2015) 535–543. doi:10.1007/s11630-015-0819-6.

[50] T. Ghisu, P. Puddu, F. Cambuli, Physical explanation of the hysteresis in Wells turbines: a critical reconsideration, ASME Journal of Fluids Engineering 133 (11). doi:10.1115/1.4033320.

[51] T. Ghisu, P. Puddu, F. Cambuli, A detailed analysis of the unsteady flow within a Wells turbine, Proceedings of the Institution of Mechanical Engineers Part A Journal of Power and Energy 231 (3) (2017) 197–214.

[52] T. Ghisu, P. Puddu, F. Cambuli, I. Virdis, On the hysteretic behaviour of Wells turbines, Energy Procedia 126 (2017) 706–713. doi:10.1016/j.egypro.2017.08.303.

[53] T. Ghisu, F. Cambuli, M. Mandas, P. Puddu, P. Seshadri, G. T. Parks, Numerical evaluation of entropy generation in isolated airfoils and Wells turbines, Meccanica 53 (14) (2018) 3437–3456. doi:10.1007/s11012-018-0896-1.

[54] T. Ghisu, F. Cambuli, P. Puddu, I. Virdis, M. Carta, Discussion on "Unsteady RANS simulations of Wells turbine under transient flow conditions" by Hu and Li, ASME Journal of Offshore Mechanics and Arctic Engineering.

[55] C. Freitas, Journal of fluids engineering editorial policy statement on the control of numerical accuracy, Journal of Fluids Engineering, Transactions of the ASME 115 (3) (1993) 339–340. doi:10.1115/1.2910144.

[56] Editorial policy statement on numerical and experimental accuracy, AIAA Journal 52 (1) (2014) 16. doi:10.2514/1.J053252.

[57] Editorial policy statement on numerical and experimental accuracy, Journal of Aircraft 47 (1) (2010) 7. doi:10.2514/1.48594.

[58] M. Folley, T. Whittaker, The Effect of Plenum Chamber Volume and Air Turbine Hysteresis on the Optimal Performance of Oscillating Water Columns, in: 24th International Conference on Offshore Mechanics and Arctic Engineering (OMAE 2005), 2005, pp. 493–498. doi:10.1115/omae2005-67070.

[59] A. Corsini, F. Rispoli, Modeling of wave energy conversion with an oscillating water column device, in: Proceedings of the 6th European Seminar OWEMES, Brindisi, Italy, 2006, pp. 1–11.

[60] C.-P. Tsai, C.-H. Ko, Y.-C. Chen, Investigation on performance of a modified breakwater-integrated owc wave energy converter, Sustainability 10 (3) (2018) –. doi:10.3390/su10030643.

[61] E. O. Doebelin, D. N. Manik, Measurement Systems: Application and Design, 5th Edition, McGraw-Hill series in Mechanical Engineering., Tata McGrawHill Education, New Delhi, 2007.

[62] T. J. Gratton, T. Ghisu, G. T. Parks, F. Cambuli, P. Puddu, Optimization of blade profiles for the Wells turbine, Ocean Engineering 169 (2018) 202–214. doi:10.1016/j.oceaneng.2018.08.066.

[63] T. Setoguchi, M. Takao, S. Santhakumar, K. Kaneko, Study of an impulse turbine for wave power conversion: Effects of Reynolds number and hub-to-tip ratio on performance, ASME Journal of Offshore Mechanics and Arctic Engineering 126 (5). doi:10.1115/1.1710868.

[64] A. D. O. Falcão, The shoreline OWC wave power plant at the Azores, in: Proceedings of the 12th International Offshore and Polar Engineering Conference (ISOPE), no. December, 2000, pp. 42–48.

[65] C. B. Boake, T. J. T. Whittaker, M. Folley, H. Ellen, Overview and Initial Operational Experience of the LIMPET Wave Energy Plant, in: Proceedings of the 12th International Offshore and Polar Engineering Conference (ISOPE), Kyushu, Japan, 2002, pp. 586–594.

[66] Y. Torre-Enciso, I. Ortubia, L. I. López de Aguileta, J. Marqués, Mutriku Wave Power Plant: from the thinking out to the reality, in: Proceedings of the 8th European Wave and Tidal Energy Conference (EWTEC), Uppsala, Sweden, 2009, pp. 319–328.

[67] C. Josset, A. H. Clément, A time-domain numerical simulator for oscillating water column wave power plants, Renewable Energy 32 (8) (2007) 1379–1402. doi:10.1016/j.renene.2006.04.016.

[68] M. Amundarain, M. Alberdi, A. Garrido, I. Garrido, J. Maseda, Wave Energy Plants: Control Strategies for Avoiding the Stalling Behaviour in the Wells Turbine, Renewable Energy 35 (12) (2010) 2639–2648. doi:10.1016/j.renene.2010.04.009.

[69] D. Bull, J. Erick, Optimal resistive control strategy for a floating OWC device, in: 2013 10th European Wave and Tidal Energy Conference, Technical Committee of the European Wave and Tidal Energy Conference, 2017.

[70] D. Ramirez, J. P. Bartolome, S. Martinez, L. C. Herrero, M. Blanco, Emulation of an owc ocean energy plant with pmsg and irregular wave model, IEEE Transactions on Sustainable Energy 6 (4) (2015) 1515–1523. doi:10.1109/TSTE.2015.2455333.

[71] S. K. Mishra, A. Patel, Wells turbine modeling and pi control scheme for owc plant using xilinx system generator, in: 2017 4th International

Conference on Power, Control Embedded Systems (ICPCES), 2017, pp. 1–6. doi:10.1109/ICPCES.2017.8117639.

[72] A. Rizzi, J. Vos, Towards estabilishing credibility in Computational Fluid Dynamics simulations, AIAA Journal 36 (5) (1998) 668–674. doi:10.2514/2.442.